12th International Symposium on Turbulence and Shear Flow Phenomena (TSFP12)
Osaka, Japan (Online), July 19–22, 2022

PASSIVE SCALAR MIXING ENHANCEMENT AND MULTI-STRUCTURE TURBULENCE DOWNSTREAM OF A GRID AND A POROUS OBSTRUCTION

Dana Duong
Department of Mechanical Engineering
University of Ottawa
Ottawa, ON K1N 6N5, Canada
dduon101@uottawa.ca

Stavros Tavoularis
Department of Mechanical Engineering
University of Ottawa
Ottawa, ON K1N 6N5, Canada
stavros.tavoularis@uottawa.ca

ABSTRACT

Turbulent diffusion and mixing of heat, introduced passively by a thin ribbon in grid-generated turbulence, was enhanced drastically by a small array of thin cylinders, positioned closely downstream of the ribbon. A multi-structure flow region with an increasing dissipation parameter was formed behind the array and relaxed towards grid turbulence, albeit maintaining a turbulence intensity and an integral length scale that were twice as large as those in the absence of the array.

INTRODUCTION

Turbulent mixing and diffusion of scalar properties, such as heat and the concentration of an admixture, have been studied extensively, due to their importance in combustion, chemical reactions, spreading of pollutants and transmission of airborne pathogens. Much of our understanding of these phenomena has been based on studies under idealised conditions, but such findings are also relevant to many practical conditions. Early studies of scalar dispersion from concentrated sources in homogeneous turbulence (Taylor, 1922; Batchelor, 1949) have been adapted to estimate the far-field half-width of a scalar plume, generated by a line source in a uniform stream, as

$$\sigma \approx (2u_2' L_2 x_1/\overline{U}_1)^{1/2} \text{ for } \sigma \gg L_2 \tag{1}$$

where x_1 is the distance from the source, $\overline{U}_1$ is the mean velocity, u_2' is the standard deviation of the transverse turbulent velocity and $L_{22,2}$ is the transverse integral length scale. More recently, scalar diffusion theory was extended to account for turbulence decay, as would be the case for grid-generated turbulence (Tavoularis & Nedić, 2017). In this case, the far-field plume half-width was estimated as

$$\sigma \propto C_\varepsilon^{-1/2} L_1 \tag{2}$$

where L_1 is the streamwise integral length scale and the turbulent kinetic energy dissipation parameter is defined, in terms of L, the turbulent kinetic energy per unit mass k and its dissipation rate ε, as $C_\varepsilon = \varepsilon L/(2k/3)^{3/2}$. Considering that, in grid turbulence, there is a flow region near the grid, where C_ε grows monotonically and beyond which $C_\varepsilon \approx$ const. (Tavoularis & Nedić, 2017), Eq. 2 implies that, if the far-field condition ($\sigma \gg L$) is satisfied at the start of the $C_\varepsilon \approx$ const. region, it will continue being satisfied further downstream, so that the plume will grow at the same rate as the turbulence scale does. The analysis also indicates that, if the far-field condition is not satisfied at the start of the $C_\varepsilon \approx$ const. region, it will never be satisfied and the plume will keep growing at a slower rate than L does. The previous observations lead to the following strategy for enhancing the spreading of the plume, thus improving scalar mixing in decaying grid turbulence: introduce a disturbance close to the source, so that the plume will be wide enough as to satisfy the far-field condition early in its evolution and then keep growing at its highest possible rate, which is the rate of growth of L. The crucial step is to implement this strategy as efficiently as possible. Introducing a relatively large solid obstruction in the plume would spread the plume, but would also create a large wake, where the turbulence structure would be very different from grid turbulence and the analysis would not hold, even approximately. Moreover, the scalar released by the source may take considerable distance to be entrained in the wake. After considering different possibilities, we decided to use an array of small cylinders, which would act like a porous obstruction, thus allowing the scalar to penetrate the array as well as reducing the disturbance to the grid turbulence. Of course, the turbulence structure behind the array would have contributions from the upstream grid turbulence, as well as contributions of the wakes of the cylinders and the high-speed flows between them. Consequently, this region will have a structure that is the result of more than one distinct turbulence generation mechanisms and may be described as *multi-structure turbulence* (Nedić & Tavoularis, 2018).

In a recent article, Nedić & Tavoularis (2016) showed that decaying grid turbulence has three distinct regions, namely, a developing region, a partially developed region, and a fully

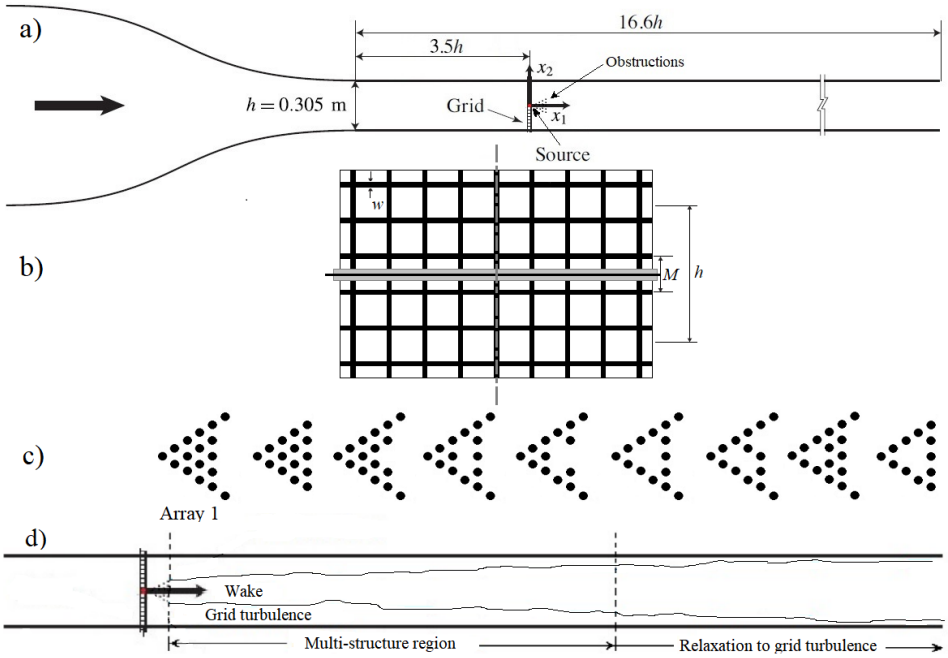

Figure 1: Sketches of a) the general experimental arrangement, b) a front views of the perforated plate (thick black lines), the obstruction frontal area (Grey rectangle) and the heating ribbon (black horizontal line), c) the different cylinder arrays and d) the different flow regions.

developed region, and that the streamwise extent of each region depends on the shape and the mesh size of the grid. An important finding for the present purposes is that, in the developing region, C_ε grows monotonically, before approaching an asymptote in the fully developed region. These authors also found that, for sufficiently small mesh sizes, the developing region is essentially non-existent. This implies that the choice of grid is crucial in satisfying the far-field condition. Among the many available grids in our laboratory, the one that had the smallest mesh, but also a developing region, was found to be a square-mesh perforated plate with a mesh size $M = 50.8$ mm.

The general goal of this research is to devise a practical method for enhancing scalar mixing in a turbulent flow. In particular, we wished to widen the plume generated by a scalar line source in grid turbulence by inserting a porous obstruction closely behind it. We also wished to explore the relationship between the plume spread and the turbulence properties in the multi-structure region behind the obstruction.

APPARATUS AND MEASUREMENT PROCEDURES

The experiments were performed in an open-circuit wind tunnel, shown schematically in Fig. 1a. The test section has a height $h = 305$ mm, a width of $1.5h$ and a length of $16.6h$. A square-mesh perforated plate ("grid", shown in Fig. 1b), machined from a 16 gauge steel sheet with a thickness of 1.59 mm and having a mesh size $M = 50.8$ mm ($= 0.167h$) and a solid bar width $w = 6.8$ mm (namely, a solidity of 0.25), was inserted across the flow. An electrically heated ribbon, made of Nichrome alloy and having a thickness of 0.13 mm and a width of 1.59 mm, was inserted at a location that was 25.4 mm ($= 0.50M$) downstream of the grid, to serve as the source of a passive scalar (*i.e.*, temperature rise); the heating power was the same for all reported tests. Arrays of ceramic rods, 3.2 mm in diameter and spaced by 5.5 mm, centre-to-centre, in equilateral arrangements, were positioned 38 mm ($= 0.75M$) downstream of the source, namely, about $1.25M$ downstream of the grid. Tests were performed for nine array configurations, shown in Fig. 1c. The test section side walls past the cylinder array were adjusted to be slightly diverging, to compensate the pressure field for boundary layer growth.

Measurements of the streamwise and transverse (*i.e.*, vertical) velocity components and the fluctuating temperature were made with a home-made, three-wire probe. The velocity sensors, arranged in a cross-wire configuration, were made of tungsten and had a diameter of 2.5 μm, a sensing length of 0.85 mm and a separation distance of 0.5 mm. The length-to-diameter ratio was 340, which is sufficiently large for end conduction effects to be negligible. The temperature sensor (cold wire) was made of platinum and had a diameter of 0.6 μm and a length-to-diameter ratio of 800; this sensor was etched from Wollaston wire and spot-welded onto the prongs. The cold wire was supplied with a current of 0.3 mA by a low-noise, high-gain homemade circuit. The mean temperature close to the three-wire probe was measured with a miniature thermistor. The hot-wire signals were corrected for temperature effects, using an instantaneous temperature value that was the sum of the time-averaged temperature, measured with the thermistor, and the mean-free temperature fluctuation, measured with the cold wire. The reported temperature rise in the heated flow was the difference between the locally measured temperature and the temperature upstream of the heated source, measured with a pre-calibrated resistance temperature detector (RTD). The hot-wire and cold-wire signals were low-pass filtered with analog filters, having cutoff frequencies of, respectively, 14 kHz, and 4 kHz, digitised at a rate of 30 kHz and recorded over 30 s for each test. The cross-wire probe was calibrated *in situ* using a velocity-pitch-map calibration method.

The streamwise integral time scale T_1 was determined by integrating the temporal autocorrelation coefficient of the streamwise velocity fluctuations to its first zero-crossing. The streamwise integral length scale was then estimated as $L_1 =$

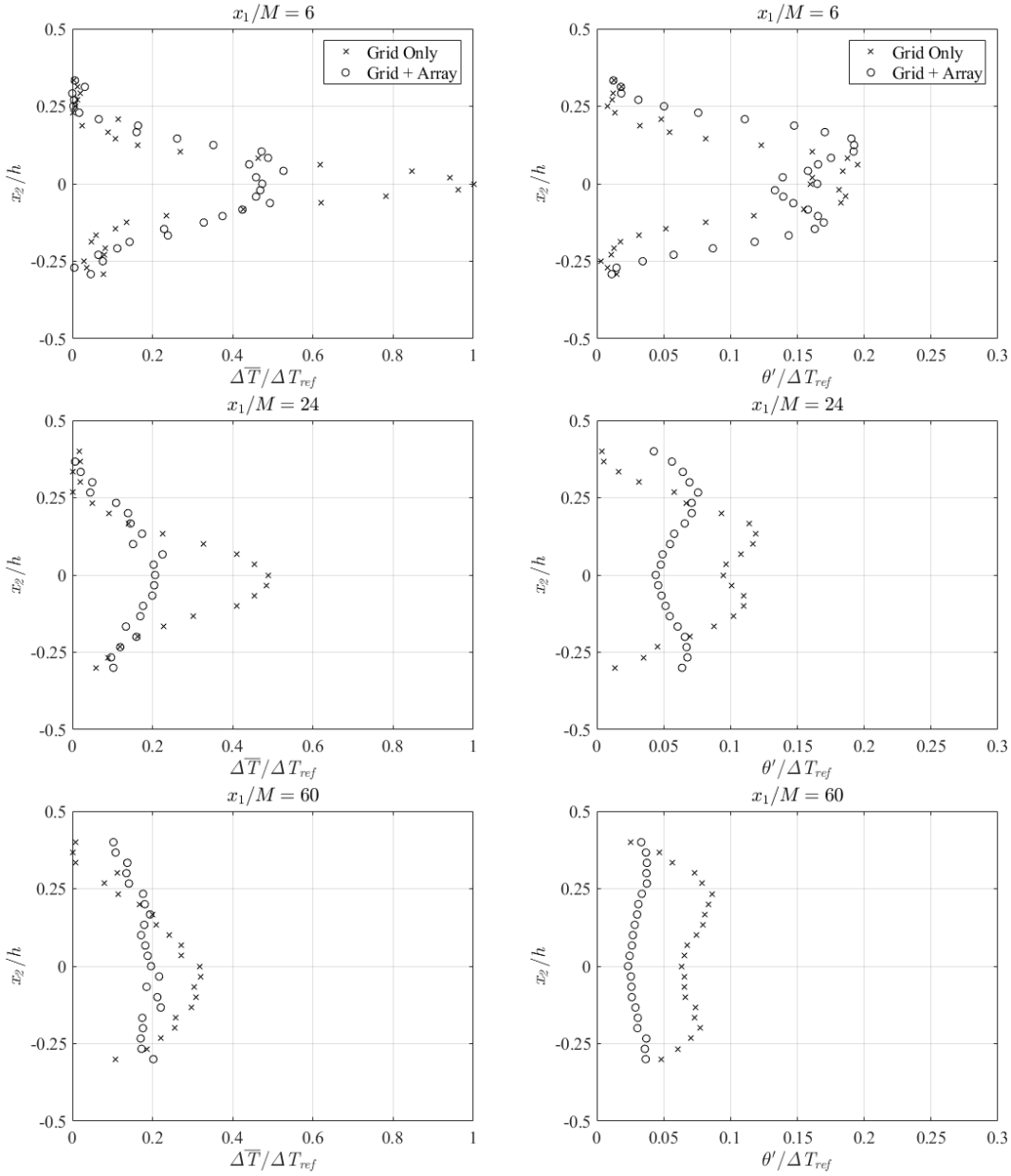

Figure 2: Normalised mean temperature and temperature fluctuation profiles without and with the obstructions at three downstream locations; the reference temperature rise was $\Delta T_{ref} = 0.44$ K.

$T_1\overline{U}_1$. The derivative $\overline{(\partial u_1/\partial t)^2}$ was calculated by extrapolating corresponding finite differences to a zero time lag. Using Taylor's frozen flow approximation, the Taylor microscale was calculated as $\lambda = \overline{U}_1\left[u_1'^2/\overline{(\partial u_1/\partial t)^2}\right]^{1/2}$, the turbulence Reynolds number was calculated as $\mathrm{Re}_\lambda = u_1'\lambda/\nu$, where ν is the kinematic viscosity of air, and the turbulent kinetic energy dissipation rate was estimated as $\varepsilon = 15\nu u_1'^2/\lambda^2$. The Kolmogorov microscale was then calculated as $\eta = \left(\nu^3/\varepsilon\right)^{1/4}$ and the dissipation parameter was calculated as $C_\varepsilon = (L_1\varepsilon)/u_1'^3$. Lastly, the Taylorian diffusivity was calculated as $D = u_2'^2 L_1/2$.

RESULTS AND DISCUSSION

All measurements were taken at a fixed inlet velocity of $U_\infty = 10.0$ m/s, calculated from the mean pressure difference across the wind tunnel contraction. In the absence of flow obstructions, velocity fluctuations in the streamwise and transverse directions were found to be about 0.1%. The Reynolds number, based on the grid mesh size, was $Re_M = U_\infty M/\nu \approx 34{,}000$.

Preliminary measurements downstream of each of the nine cylinder arrays showed that, in general, the mean temperature profiles had a nearly Gaussian shape, with a peak that was substantially lower than that in unobstructed grid turbulence, while the plume was substantially wider. The additional spread of heat in the presence of the obstruction is attributed to two interacting, but distinct, effects. First, the warm wake of the source is either split by the first cylinder or diverted towards one side of it, in both cases tending to displace heated fluid away from the source plane. This process is repeated, as the displaced warm fluid reaches the second and subsequent cylinders. One is also reminded that the near field of a square-mesh grid consists of square jets, surrounded by short horizontal and vertical wakes, so that the flow reaching the ob-

struction is strongly three-dimensional. Second, the cylinders produce additional turbulent fluctuations, which are superimposed on the grid turbulence, as well increasing the size of the energy containing motions; both effects enhance turbulent diffusion. The effect of the obstructions on the plume spread is quite strong, despite the fact that the frontal projection of a full cylinder array is merely $0.076h$ in height.

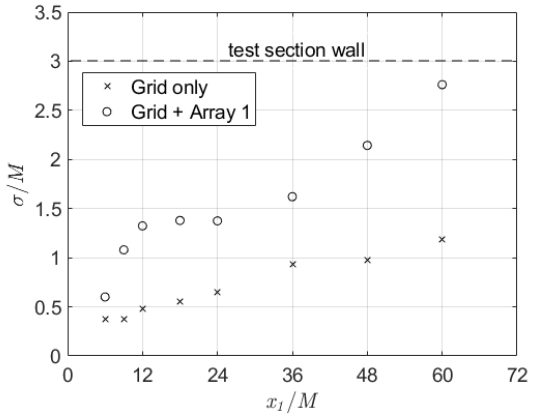

Figure 3: Plume spread without and with the obstructions.

Most effective in reducing the peak temperature rise was Array 1, so all measurements reported here were taken for this configuration. Profiles of the mean temperature rise $\Delta\overline{T}$ at three streamwise stations are shown in Fig. 2. These values have been normalised by a constant reference temperature rise $\Delta T_{ref} = 0.44$ K, which is equal to the peak mean temperature rise in the unobstructed flow at $x_1/M = 6$. Although the unobstructed plume extended entirely within the flow core region (namely, it did not reach the boundary layers along the top and bottom walls), the obstructed plume grew wider than the core, encroaching into the boundary layers at the furthest station, where $x_1/h = 10$. Fig. 2 also presents the transverse profiles of the normalised standard deviation θ' of the temperature fluctuations, at the same three streamwise locations. Dual peaks can be seen in both the unobstructed and obstructed flows, but, in the obstructed flow, the fluctuations spread further in the transverse direction and had a smaller non- uniformity. As shown in Fig. 3, the obstructed plume was roughly twice as wide as the unobstructed one. The same figure indicates that the obstruction intensified scalar mixing to the point that, roughly speaking, the mean temperature rise in the entire test section far away from the source exceeded half of its peak value. In contrast, throughout the unobstructed flow, there were significant parts of the test section, where there was no temperature rise at all. All things considered, we may confidently assert that the obstruction was quite effective in spreading and mixing the scalar.

To understand the effect of the obstructions, we compared the turbulence properties in their presence with those in their absence. Representative results are shown in Fig. 4. It should be noted that the various profiles near the grid are not expected to be two-dimensional, but to have significant spanwise non-uniformity, generated by the vertical bars of the grid. It is also noted that the heating ribbon, which was given a small twist, had a measurable momentum wake, although we found no signs of buoyancy effects due to the heating. The results may be summarised as follows.

(a) Closely downstream of it, the obstruction increased the mean velocity deficit along the centreline to a level that was well above the already significant level in the absence of the obstruction, which is attributed to the grid bars and the ribbon wake. This deficit diminished with downstream distance, so that the mean flow in the core became nearly uniform at $x_1/M = 60$. At that location, the boundary layers on the top and bottom walls may be seen to occupy roughly a quarter of the cross-section each, with very weak velocity peaks persisting at the boundary layer edges; these peaks are interpreted to be remnants of upstream flow maxima between bar-generated wakes.

(b) The streamwise turbulent velocity fluctuation level behind the obstruction was nearly twice the unobstructed value in the entire test section, which means that the obstruction generated a permanent increase in turbulence level.

(c) The transverse turbulent velocity fluctuations behind the obstruction followed the same overall patterns as the streamwise fluctuations. It is interesting to note that, at $x_1/M = 6$, u_2' was somewhat larger than u_1', as the obstruction diverted flow away from the centreline. Further downstream, the ratio u_1'/u_2', both without and with obstructions, settled at a level in the range $1.1 - 1.2$, which is somewhat larger than typical values in turbulence generated by grids with solidities that are higher than the present one (Comte-Bellot & Corrsin, 1966).

(d) The shear stress correlation coefficient was only mildly affected by the obstruction. It is interesting to note that, without and with the obstruction, this coefficient had peaks of about ± 0.25, which points to a persisting mild anisotropy throughout the measuring section. This is attributed to the relatively small solidity of the grid and the limited streamwise distance available in the present test section for the flow anisotropy to diminish further.

(e) The obstruction nearly doubled the integral length scale, and such increase was maintained downstream.

(f) The obstruction increased drastically the turbulent diffusivity $D \approx u_2'^2 L_1/2$ in its wake. Close to the obstruction, the increase was by an order of magnitude and peaked on the centreline, but, further downstream, the turbulent diffusivity maintained a fairly uniform value in the flow core, which was roughly four times the corresponding unobstructed value. This increase in D is consistent with the drastic enhancement of scalar mixing.

(g) The Taylor microscale was essentially unaffected by the obstruction; this indicates that the obstruction increased both the velocity fluctuations and their temporal derivative by the same amount. Nevertheless, there was a very small correlation ($\lesssim 0.1$ for $x_1/M \geq 24$) between the velocity and its derivative. A physical justification for the lack of influence of the obstruction on the Taylor microscale remains to be found.

(h) The turbulence Reynolds number was roughly doubled by the obstruction, as a result of the increase of the turbulence level.

(i) The dissipation rate was nearly tripled close to the obstruction and maintained a comparable increase in the entire test section, while its level diminished rapidly.

(j) The dissipation parameter was significantly reduced by the obstruction, with the reduction diminishing with distance from the obstruction and vanishing far downstream.

These results support the expectation that the wake of the overall obstruction was a multi-structure region, which tended

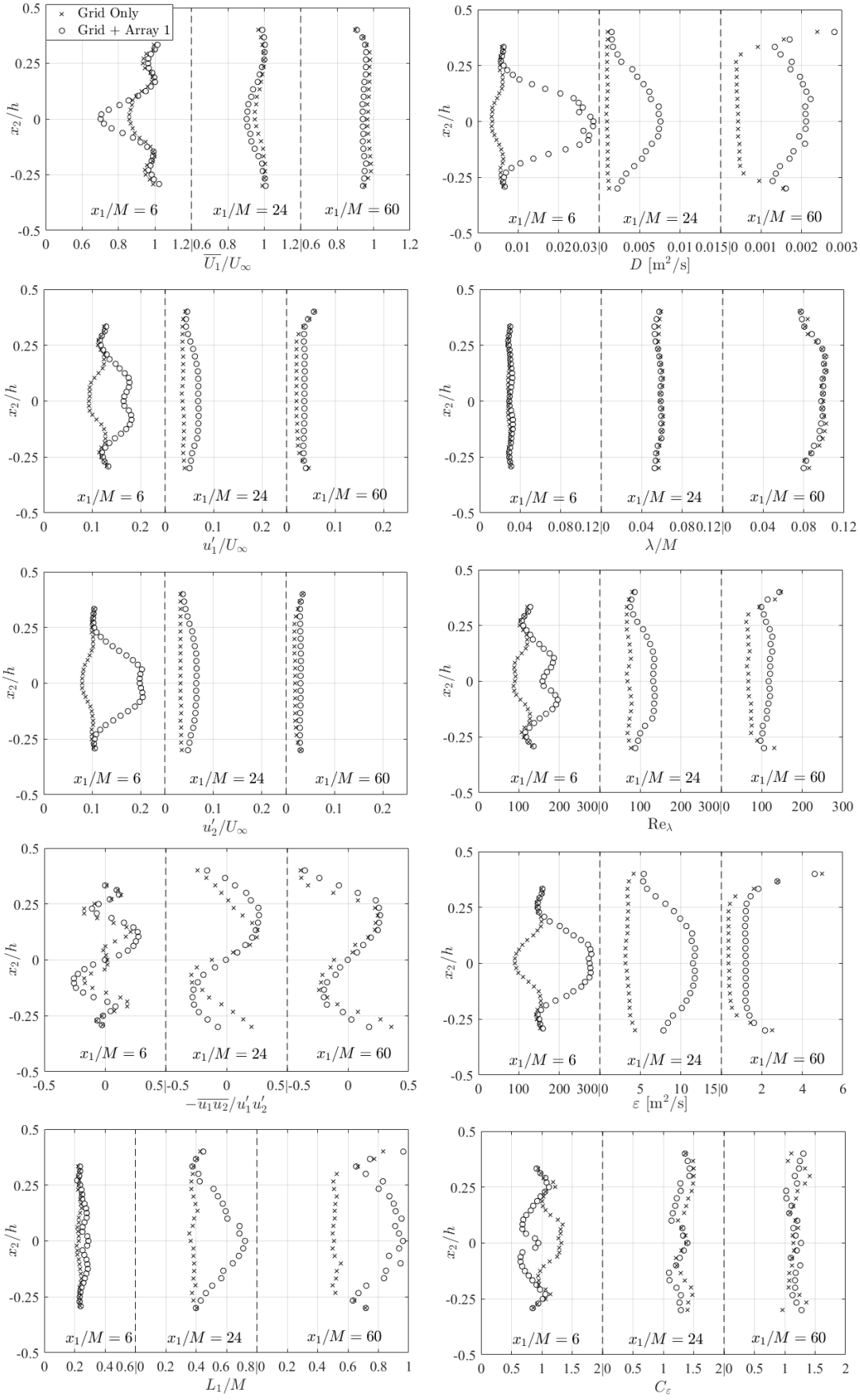

Figure 4: Transverse profiles of the main turbulence properties at three representative streamwise locations; the axis scales for L_1, D and ε at the three streamwise locations have been adjusted to make the values in the plots readable.

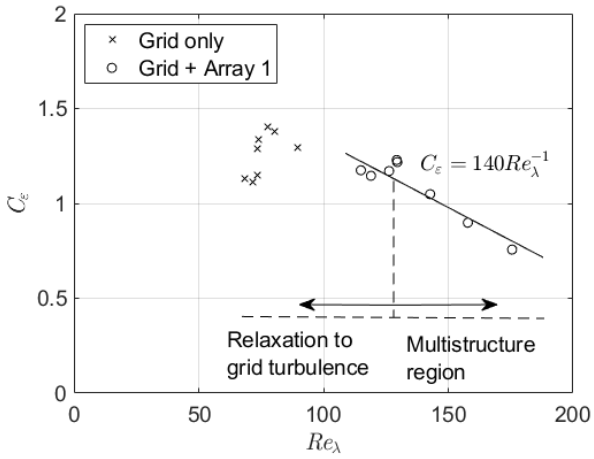

Figure 5: Dissipation parameter *vs.* the turbulence Reynolds number.

to relax to grid turbulence, albeit maintaining a permanent and significant increase in the turbulence intensity and integral length scale (see flow regions in Fig. 1d). An important finding that deserves further attention is that, as shown in Fig. 5, the dissipation parameter in the multi-structure region was inversely proportional to the local turbulence Reynolds number. Such a relationship has also been observed between these two parameters in multi-structure regions of other flows, including intermediate regions of decaying grid turbulence (Vassilicos, 2015; Nedić & Tavoularis, 2016), uniformly sheared turbulence disturbed by a grid (Nedić & Tavoularis, 2018), early stages of turbulent boundary layers (Nedić *et al.*, 2017) and a turbulent boundary layer in a uniformly sheared free stream (Livingston & Tavoularis, 2022).

As a final note, Fig. 6 shows representative profiles of the skewness S and flatness F factors of the streamwise velocity derivative, which are indicators of the fine structure. Away from the grid ($x_1/M \geq 24$), S takes values in the vicinity of -0.5 in both the unobstructed and the obstructed flows; such values are typical for fully developed turbulence at moderate Reynolds numbers. However, closer to the grid ($x_1/M = 6$), S takes values that are measurably lower than the value -0.5 without the obstruction and closer to -0.5 with the obstruction; thus, it appears that the effect of the obstruction is to accelerate the development of the fine structure. Moreover, the obstruction increases systematically K throughout the test section, which is consistent with the increase in Re_λ and indicates an enhancement of the internal intermittency of the turbulence.

CONCLUSIONS

In this experimental work, we found that a small array of thin cylinders, acting as a localised, porous, flow obstruction, enhanced drastically turbulent diffusion and mixing of a passive scalar injected from a line source in grid turbulence. The unobstructed scalar plume was confined within the test section core region, whereas the obstructed plume penetrated the boundary layers on the test section walls. This is further confirmed by the fact that the plume spread in the obstructed flow was twice as large as that in unobstructed grid turbulence. Transverse profiles of turbulence properties indicated that a multi-structure flow region was formed behind the array and relaxed towards grid turbulence, albeit maintaining permanent

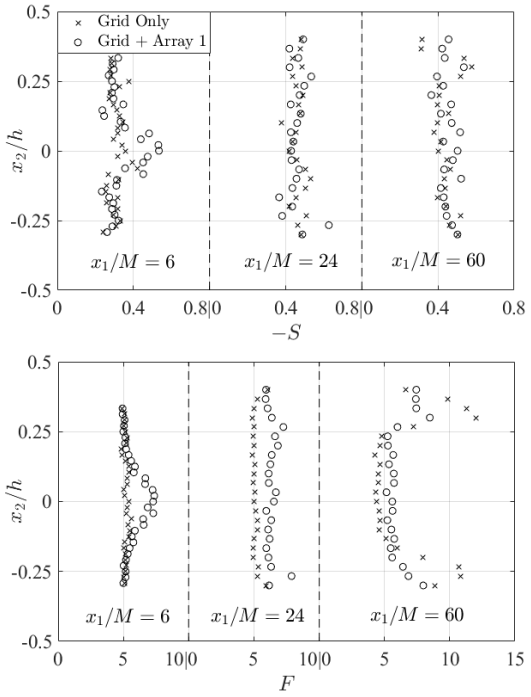

Figure 6: Transverse profiles of the skewness and flatness factor of the streamwise velocity derivative. The axis scale of F at the last streamwise location has been adjusted to make the values in the plot readable.

increases in turbulence level, integral length scale and turbulent diffusivity.

Funding for this research was provided by the Natural Sciences and Engineering Research Council of Canada.

REFERENCES

Batchelor, G.K. 1949 Diffusion in a field of homogeneous turbulence. I Eulerian analysis. *Austral. J. Chem.* **2**, 437–450.

Comte-Bellot, G. & Corrsin, S. 1966 The use of a contraction to improve the isotropy of grid-generated turbulence. *J. Fluid Mech.* **25**, 657–682.

Livingston, C. & Tavoularis, S. 2022 Multi-structure turbulence in a boundary layer with a uniformly sheared free stream. In *Proc. TSFP12, Osaka, Japan, July 19–22, 2022*, pp. 1–6.

Nedić, J. & Tavoularis, S. 2016 Measurements of passive scalar diffusion downstream of regular and fractal grids. *J. Fluid Mech.* **800**, 358–386.

Nedić, J. & Tavoularis, S. 2018 A case study of multi-structure turbulence: Uniformly sheared flow distorted by a grid. *Int. J. Heat Fluid Flow* **72**, 233–242.

Nedić, J., Tavoularis, S. & Marusic, I. 2017 Dissipation scaling in constant-pressure turbulent boundary layers. *Phys. Rev. Fluids* **2** (3), 032601.

Tavoularis, S. & Nedić, J. 2017 Taylorian diffusion in mildly inhomogeneous turbulence. *Intern. J. Heat Fluid Flow* **67**, 116–121.

Taylor, G. I. 1922 Diffusion by continuous movements. *Proc. Roy. Soc. London. Series A* **151** (873), 196–212.

Vassilicos, J. C. 2015 Dissipation in turbulent flows. *Annu. Rev. Fluid Mech.* **47** (1), 95–114.